Calculated Structural and Electronic Interactions of the Ruthenium Dye N3 with a Titanium Dioxide Nanocrystal

Petter Persson* and Maria J. Lundqvist

Department of Quantum Chemistry, Uppsala University, Box 518, SE-751 20 Uppsala, Sweden

Received: January 29, 2005; In Final Form: April 2, 2005

Structural and electronic properties of a small anatase TiO_2 nanocrystal sensitized by the ruthenium dye N3 ($Ru(4,4'$-dicarboxy-$2,2'$-bipyridine$)_2(NCS)_2$) have been investigated using density functional theory (DFT) with support from Hartree−Fock (HF) and time dependent DFT (TD-DFT) calculations. Significant structural adjustments of both the dye and the nanocrystal are predicted to be induced by the strain imposed by the simultaneous formation of multiple dye−surface bonds. Electronic properties of the combined dye−nanocrystal system have also been calculated, including information about interfacial orbital mixing and the lowest excited singlet states. Ultrafast photoinduced electron transfer processes across the dye−nanoparticle interface in dye-sensitized solar cells are finally discussed in view of estimated electronic coupling strengths. The calculations predict injection times on the order of 10 fs for MLCT excitations to the ligand π^* levels that interact most strongly with the TiO_2 conduction band, and an order of magnitude increase in the injection times for excitations to dye levels with poor spatial or energetic overlaps with the substrate conduction band.

Introduction

Dye-sensitized nanostructured TiO_2 electrodes are capable of efficient charge separation across the dye−metal oxide interface under illumination with visible light.[1] This is a central feature of a promising class of photovoltaic devices including so-called dye-sensitized solar cells.[2,3] Following an initial excitation of a dye molecule by incident light, the photoexcited electron can be rapidly injected from the dye into the conduction band of the TiO_2 particle. Such photoinduced electron-transfer processes have been measured for a variety of systems and can under favorable conditions proceed on a sub-100 fs time scale.[4−9] The efficiency of the charge separation is central to the performance of dye-sensitized solar cells and needs to be faster than competing loss processes, such as regeneration of the ground state of the dye.[2,10] Dye-sensitized semiconductor interfaces, and in particular photoinduced heterogeneous electron injection mechanisms occurring at these interfaces, have therefore been investigated intensively over the last 15 years, primarily using a range of experimental electrochemical and photochemical techniques.[2,7] Because of their complexity, many details of the dye−nanoparticle structural and electronic interactions are, however, still not well-understood. This includes, for example, realistic atomistic models of typical dye−surface binding modes, as well as questions about how the interfacial electronic properties are related to those of the separate components. For example, it is generally assumed that the structure and electronic properties of the dye molecules remain essentially unaltered on binding to a substrate. This is supported by the fact that there typically only are minor changes between absorption spectra of free and surface-attached ruthenium dyes. There are, however, examples for which the long-term stability of the dye−semiconductor interfaces,[11,12] or the absorption spectra of the photoinduced electron transfer, can be quite sensitive to local properties of the interface. For example, there is a significant adsorption induced shift, ascribed to direct sensitizer-to-semiconductor charge-transfer excitations in the absorption spectrum of the organic sensitizer catechol.[13−15] Evidence for adsorption-induced changes to the adsorbate electronic properties has also been provided by combined NEXAFS and computational investigations of the $4,4'$-dicarboxy-$2,2'$-bipyridine (dcb) binding ligand on different TiO_2 surfaces.[16,17]

Nanostructured TiO_2 sensitized by so-called N3 dyes ($Ru(4,4'$-dicarboxy-$2,2'$-bipyridine$)_2(NCS)_2$) is probably the most well-known example of a dye-sensitized nanocrytalline metal oxide semiconductor and has been the subject of numerous experimental investigations.[2,3,7,18,19] The N3 and related ruthenium dyes have consequently also been subject to a number of quantum chemical investigations,[20] elucidating aspects of, for example, the basic molecular orbital structure and excited-state properties.[21] Several theoretical investigations employing the density functional theory (DFT) level of theory have recently been published.[22−26] Together, these studies have shown that calculations are useful for analyzing the molecular orbital compositions and excited states of the dyes used in ruthenium dyes commonly used in dye-sensitized solar cells under various solvent and pH conditions.

Accurate calculations of heterosupramolecular systems including organic and organometallic dyes bound to metal oxide substrates such as nanocrystalline TiO_2 have only recently started to become possible.[20] Calculations have been presented both for organic sensitizers, such as catechol, quinizarin, and alizarin,[20,27−30] and the organometallic sensitizer $[Fe(CN)_6]^{4-}$.[31] Theoretical models of the adsorption of ruthenium dyes on TiO_2 substrates have been presented based on structural matching,[32] calculations of the binding of anchor groups[33] and binding ligands of Ru dyes,[20,34−36] and for ruthenium dye binding to a small TiO_2 cluster.[37] Dynamical aspects of photoinduced heterogeneous electron-transfer processes have also been investigated theoretically (e.g., by Willig and co-workers).[38] Electronic structure based calculations based on electron coupling,[39] nonadiabtatic molecular dynamics,[40] and electron

* To whom correspondence should be be addressed. Phone: 46 18 471 35 79; fax: 46 18 471 58 30; e-mail: Petter.Persson@kvac.uu.se.

10.1021/jp050513y CCC: $30.25
Published on Web 05/27/2005

dynamics[28] approaches have been tested for predictions of heterogeneous electron-transfer rates on model systems.

To correctly account for the effect that surface traps and quantum size effects might have on the structural and electronic properties of dye-sensitized nanocrystalline materials, we have recently started to make systematic investigations of TiO_2 nanocrystals.[41] Such nanocrystals also provide suitable substrates for calculations of dye-sensitized TiO_2 nanocrystals.[20,13,31]

Here, we present DFT calculations of a prototypical N3−TiO_2 nanocrystal interface, together with complementary Hartree−Fock (HF) and time-dependent DFT (TD-DFT) calculations. A complete DFT geometry optimization of a preselected binding mode provides information about interfacial structural modifications of the dye and nanocrystal, and a detailed analysis of the electronic structure in terms of the Kohn−Sham molecular orbitals (MOs) at the optimized geometry was used to provide information about the electronic interactions at the interface. The electronic structure information together with TD-DFT calculations of the lowest excited singlet states were used to discuss the nature of different photoinduced heterogeneous electron-transfer processes occurring at these interfaces. Detailed theoretical information about these interfaces is an important prerequisite for rational improvements of the photovoltaic devices relying on charge separation at dye−semiconducor interfaces.

Materials and Methods

Full geometry optimizations and electronic structure calculations of the system comprising the N3 dye and a $(TiO_2)_{38}$ model of a TiO_2 nanoparticle were performed using the B3LYP functional. Split valence basis sets were used together with effective core potentials (ECPs). The Ru, N, and S atoms were described using the standard LANL2DZ basis set,[42] while the H, C, O, and Ti atoms were described using a basis set that we have previously found suitable for calculations of organic adsorbates on metal oxide surfaces.[20,39] In the final electronic structure calculation of the fully optimized system, an additional diffuse basis function was added to all oxygen atoms to better describe the electron density of the negatively charged oxygen atoms in the metal oxide.[39] TD-DFT calculations of the three lowest excited singlet states of the combined system were performed using the same functional and basis set as the final electronic structure calculations. The GAUSSIAN03 program[43] was used for all the calculations.

It may be worth pointing out that although it is the total ground state electron density that is primarily sought in DFT calculations, the MOs that appear in the Kohn−Sham formalism are usually remarkably similar to the canonical Hartree−Fock MOs. They are thus used routinely to provide a useful tool for qualitative analysis of chemical properties.[44] The electronic structures of ruthenium dyes,[22−26] TiO_2 solids,[45] and nanocrystals[41] as well as dye-sensititzed TiO_2[31] have in recent years all been successfully analyzed in this way. Moreover, we have also performed a Hartree−Fock (HF) calculation on the optimized N3-sensitized TiO_2 nanoparticle, using the same basis set as for the DFT calculations, and verified that the main qualitative MO shapes and relative energetics presented in terms of the Kohn−Sham orbitals are closely corroborated by the corresponding HF MOs after consideration has been taken to the fact that the HF HOMO−LUMO gap significantly overestimates the TiO_2 band gap. We are therefore confident that the presented analysis based on the Kohn−Sham orbitals is useful for an improved understanding of the electronic structure of these systems. In principle, a more complete analysis of the electronic properties of the excited states could be obtained from a calculation of a full excitation spectrum (e.g., using TD-DFT). Such approaches are, unfortunately, still too expensive computationally for dye-sensitized TiO_2 nanocrystals except for the few lowest states.[31] Here, the three lowest vertical excitations to excited singlet states were calculated using TD-DFT.

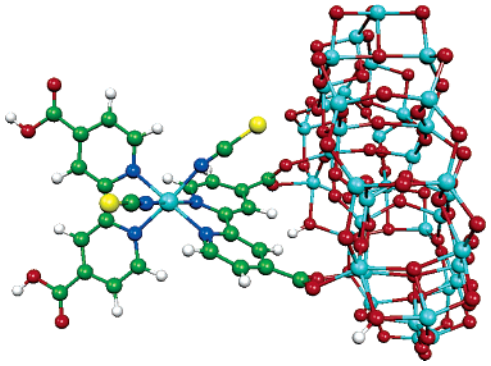

Figure 1. Fully optimized geometry of the ruthenium dye N3 (Ru(4,4′-dicarboxy-2,2′-bipyridine)$_2$(NCS)$_2$) attached to a 1.5 nm TiO_2 nanocrystal.

Results

Structure. A model of N3 bound to a $(TiO_2)_{38}$ nanoparticle was constructed starting from a model of the interface of the TiO_2 anatase (101) surfaces with one of the N3 binding ligands (4,4′-dicarboxy-2,2′-bipyridine), referred to as dcb or bi-isonicotinic acid, previously investigated theoretically.[35] In reality, several different binding modes are likely to be present simultaneously. They can be distinguished by which anchor groups are involved, the relative positions of the adsorption sites, and the binding mode of each anchor group. As the relative stability of the different binding modes is expected to depend strongly on the detailed experimental preparation conditions, we have limited this pilot investigation to a single binding mode involving two bridge-binding anchor groups on the same bi-isonicotinic acid ligand according to a suggestion from an earlier investigation of the bi-isonicotinic acid binding to an anatase (101) surface.[35] The possibility to extend the model of the bi-isonicotinic acid ligand to complete ruthenium dyes, such as N3, has been suggested previously based on the limited deformation of the chelating environment of the central ruthenium atom even when the ligand is fully relaxed on TiO_2 by itself.[20] The $(TiO_2)_{38}$ model of the nanocrystal is the same as we have used previously for studies of organic adsorbates on TiO_2 nanocrystals.[13,20] The limited diameter of this particular cluster of ca. 1.5 nm makes it difficult to simulate all possible binding modes in a realistic way. In particular, the binding modes involving anchor groups from several dcb ligands simultaneously have footprints that are large as compared to the nanocrystal surfaces. The current investigation of surface attachment via two anchor groups on a single ligand is, however, interesting in itself, both because it has recently been reported that a significant fraction of N3 dyes may indeed bind to TiO_2 films via a single dcb ligand[46] and because this binding mode also is likely to be representative for the binding of several other ruthenium dyes carrying only a single dcb anchoring ligand.[11,12,20]

The structural relaxations involved in the interaction with a TiO_2 nanoparticle were investigated by a full geometry optimization of the combined N3-$(TiO_2)_{38}$ system, with the optimized structure shown in Figure 1. Interestingly, the optimization results in a significant strengthening of the two anchor-substrate bonds at the expense of significant structural adjustments

of both the dye and the nanocrystal. The two carboxylate anchor groups of the binding ligand are twisted out of the pyridine ring planes to position the carboxylates favorably relative to the surface. The Ru−N interactions, however, largely suppress the pyridine−pyridine twist of the bound dcb that was observed for the dcb ligand binding to TiO_2 by itself.[35]

The nanocrystal undergoes significant surface relaxations as compared to its unrelaxed crystal structure to adjust to the undercoordination of many surface atoms. The optimized geometry of the combined system shows substantial additional modifications of the nanocrystal surface in the vicinity of the dye molecule. In particular, the surface titanium atoms to which N3 binds are displaced outward to positions where they interact more favorably with the N3 carboxylate oxygens. This is accompanied by relaxations also of neighboring substrate atoms. Similar to the dcb in the TiO_2 case, the binding of N3 to TiO_2 nanocrystals via multiple anchor sites is thus seen to be a compromise between optimal nanocrystal and dye geometries on one hand and strong dye−nanocrystal binding on the other hand.[20,34−36]

As the bipyridine of the binding ligand is much less twisted in the optimized N3 structure as compared to the bi-isonicotinic acid case, the whole dye is relatively free to tilt with essentially intact surface anchoring. This makes it possible to form further dye−surface contact points, which in this particular optimization resulted in a structure in which the terminal sulfur atom of one of the NCS groups ends up only about 3.5 Å from the nearest surface atoms. In a different local environment, it would seem equally plausible that this flexibility instead could result in other additional contact points, such as, for example, the formation of a third carboxylate−TiO_2 anchor point, thus introducing carboxylate anchor points on both dcb ligands of N3 simultaneously. Going beyond simple structural models, by incorporating structural relaxations and the formation of multiple anchor points, it is thus seen to be important to assess the binding of different dye−substrate combinations. In particular, these effects may help to rationalize differences in interfacial stability between related Ru dyes.[11,12]

Electronic Structure. The electronic structure of the combined system is represented in Figure 2 as an effective density of states (DOS), constructed through a Gaussian broadening of the individual orbital contributions by an arbitrary factor of 0.3 eV. The N3 contributions are shown as the adsorbate partial DOS (PDOS), obtained from the atomic orbital coefficients located on the atoms belonging to N3. The TiO_2 nanoparticle has a reasonably well-developed band structure, with a valence band, band gap, and conduction band structure. The N3 orbital structure is in many ways similar to that calculated for free dyes.[21−26] The highest few occupied and lowest few unoccupied orbitals are of particular interest, as they are believed to be involved in the optical transitions leading to photoinduced transfer of electrons from the dye to the semiconductor. Selected DFT MOs of the combined system are shown in Figure 3. The main features of the calculated DOS are confirmed by the DOS of the HF calculation presented in Figure S1 in the Supporting Information.

The few highest occupied orbitals are located near the middle of the substrate band gap and are seen, in the calculations of the combined system, to be localized on the N3 dye. For example, the highest occupied molecular orbital (HOMO) is a Ru 4d orbital that is delocalized onto the NCS ligands as shown in Figure 3a. This characteristic delocalization is consistent with results from calculations on free ruthenium dyes.[20−25] Ru(II) dyes typically have six electrons occupying three nearly

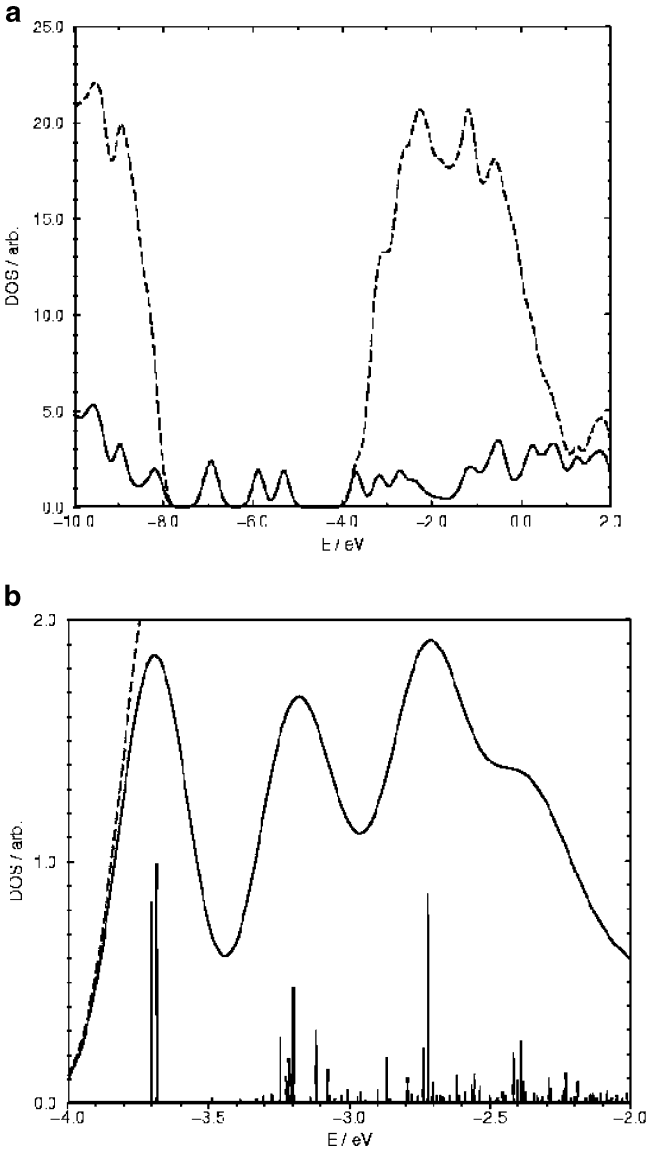

Figure 2. Calculated density of states (DOS) of N3 attached to a TiO_2 nanocrystal. (a) Total DOS (dashed curve) and N3 PDOS (solid curve). (b) Magnified view of the DOS near the conduction band edge, with lines representing the N3 PDOS contributions to individual levels. The DOS and PDOS curves were obtained using a Gaussian broadening of the individual levels by 0.3 eV. The fully occupied TiO_2 valence band (up to ca −8 eV), of which approximately the upper half is shown in panel a, is dominated by O 2p contributions, while the first part of the empty conduction band, starting at approximately −4 eV, is dominated by Ti 3d contributions. For the present $(TiO_2)_{38}$ cluster, this means that the valence and lower conduction band contain 228 and 190 electronic levels, respectively. In addition, there are more than 30 levels belonging to the N3 dye influencing the DOS in the displayed energy region.

degenerate, t_{2g} Ru 4d orbitals. For NCS containing complexes, the NCS groups contribute additional occupied orbitals in the same energy range as the t_{2g} Ru 4d orbitals, so that the HOMOs are mixed Ru−NCS orbitals.[20−25] The HOMOs of the free N3 dye are thus well-preserved for the combined system in which N3 binds to a TiO_2 nanocrystal, and there is little interaction with the substrate bands due to the poor energy matching. This is confirmed by the HF calculation.

The lowest few unoccupied dye orbitals are close in energy to the TiO_2 conduction band edge. This is shown in greater detail in Figure 2b, where the DOS plot in Figure 2a has been magnified around the conduction band edge region. In addition to the broadened total DOS and N3 PDOS, lines have been

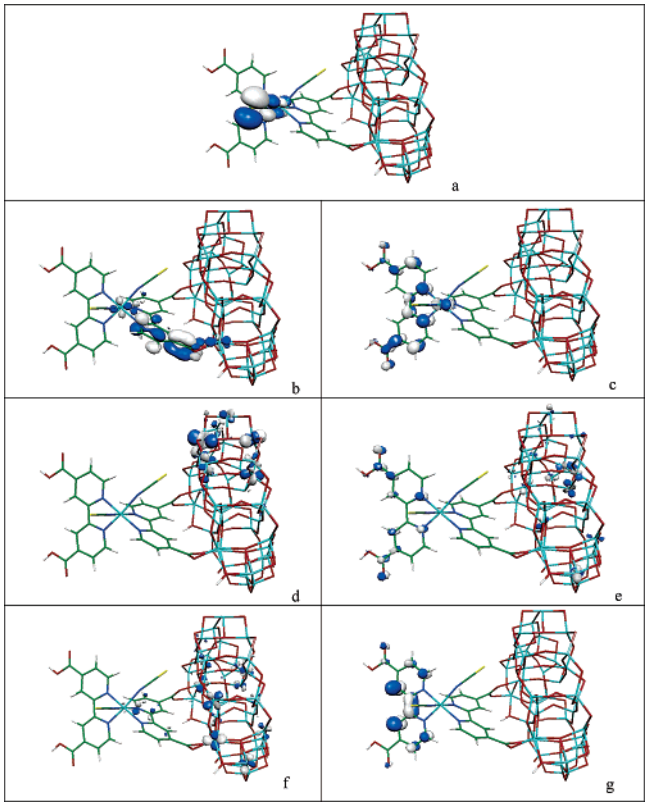

Figure 3. Molecular orbital plots of the ruthenium dye N3 attached to a TiO_2 nanocrystal: (a) mixed Ru-metal 4d and NCS-ligand π HOMO, (b) dcb-ligand π_b*(+) LUMO, (c) dcb-ligand π_b*(+) LUMO + 1, (d) TiO_2 LUMO + 2, (e) dcb-ligand π_b*(−) LUMO + 12, (f) dcb-ligand π_b*(−) LUMO + 14, and (g) dcb-ligand π_a*(+) LUMO + 31.

TABLE 1: Calculated Properties of Selected Unoccupied Molecular Orbitals[a]

MO	ϵ (eV)	ads. PDOS (%)	location	main character
LUMO	−3.70	86	anchoring dcb	π_b*(+)
LUMO + 1	−3.68	99	free dcb	π_b*(+)
LUMO + 2	−3.48	2	TiO_2	TiO_2
LUMO + 12	−3.20	48	free dcb	π_b*(−) + TiO_2
LUMO + 14	−3.12	31	anchoring dcb	π_b*(−) + TiO_2
LUMO + 31	−2.72	87	free dcb	π_a*(+)

[a] The characters of the π* orbitals located mainly on the dcb ligands are designated by a subscript describing the symmetry of the pyridine rings (a or b) with respect to rotation around the pyridine C_{2v} axis, as well as a sign signifying if the orbital has a bonding (+) or antibonding (−) interaction between the two pyridine rings.

included in the plot to indicate the location and amount (according to the PDOS analysis) of N3 contributions to the individual levels. Information pertaining to selected levels is listed in Table 1, including the orbital energies, information about the location of the orbital in the system, and the character of the orbital. A distinction is made between π* orbitals on N3 and conduction band levels in the TiO_2. On N3, a distinction is, furthermore, made between orbitals localized on the anchored and free dcb ligands. Finally, the dcb π* orbitals are distinguished, using a subscript, by the symmetry of the pyridine orbitals involved (a or b with respect to rotation about the pyridine C_{2v} axis)[39] and by a sign in parentheses, whether it is bonding (+) or antibonding (−) between the two pyridine rings.

According to the present calculations, the two lowest unoccupied molecular orbitals (LUMO and LUMO + 1) of the combined system at −3.7 eV are largely located on the two N3 dcb ligands. LUMO is a π* level located on the dcb ligand that binds to the TiO_2. According to the labeling introduced previously, it is referred to as a π_b*(+) level (see Figure 3b). It shows limited mixing with the conduction band, with the PDOS analysis given in Table 1 locating 86% of the LUMO orbital on N3, with the remaining 14% originating from the TiO_2 conduction band. The LUMO + 1 is the analogue π_b*(+) molecular orbital on the free dcb ligand that is not involved in the surface binding (see Figure 3c). This is a 99% pure N3 orbital according to the PDOS analysis in Table 1.

The two π_b*(+) levels are calculated to lie only about 0.2 eV below the conduction band edge, with the LUMO + 2 orbital at −3.48 eV being the first TiO_2 conduction band level (see Figure 3d). The energy difference between the π_b*(+) orbitals and the conduction band edge is probably too small to be decisive for determining their exact relative positions. The HF calculations also predict that there are two unoccupied MOs with ligand π* character a few tens of an eV below the conduction band edge with little substrate mixing. In the experiments published on TiO_2 sensitized by ruthenium dyes such as N3, the vertically excited lowest photoexcited singlet states are usually believed to lie above the conduction band edge by some tens of an eV[7,8] rather than a few tens of an eV below the conduction band as calculated here. It should be remembered, however, that the present calculations neglect solvent stabilization of the ground-state electronic structure that have been found to be important in recent theoretical studies of ruthenium dyes[23,24] and that the model nanocrystal probably is too small to have a completely converged bulklike band gap. This calculation therefore cannot provide a definitive answer as to the exact location of the π_b*(+) levels relative to the conduction band minimum in the experiments that have been presented for larger, solvated nanocrystals. It will therefore be important in future work to extend the present calculations to increasingly large nanocrystals and to include solvent effects until a properly quantitative agreement with experiments can be reached. Nevertheless, the nature and approximate position of these orbitals agrees reasonably well with results from previous investigations of Ru dyes[20−26] and on the dcb ligand interacting with TiO_2.[34−36] The fact that the π_b*(+) levels lie in the vicinity of the band edge is in qualitative agreement with the observation of the sensitivity to the band edge matching evidenced by the observation of both fast and slow components from the lowest excited dye states in biphasic injection rates in ultrafast photoinduced electron-transfer measurements.[8]

Above the conduction band edge, the PDOS expansion in Figure 2b shows that most levels are dominated by the TiO_2 substrate. The next higher N3 orbitals are a pair of dcb π* levels at −3.2 eV shown in Figure 3e,f. These two orbitals are antibonding combinations with respect to the pyridine−pyridine interaction of the same pyridine π_b* orbitals that made up the LUMO and LUMO + 1 orbitals. Unlike the LUMO and LUMO + 1 orbitals, however, these levels overlap the conduction band, and they can be seen in Figure 3e,f to mix strongly with the conduction band. This is reflected by the fact that no molecular orbital in the energy region from −3.5 to −3.0 eV, where these orbitals are located, has more than 48 and 31% weight on N3 for the free and anchored dcb ligand orbitals, respectively. Instead, Figure 2b indicates that the N3 PDOS contributions are spread in energy over a range of the order of 100 meV.

There is a further peak in the N3 PDOS corresponding to a sum of approximately two dye orbitals at −2.7 eV. Here, there is one π_a*(+) orbital on the free dcb ligand that only interacts weakly with the substrate, with 87% weight on N3 in the LUMO

+ 31 orbital shown in Figure 3g. The corresponding orbital on the binding dcb ligand is, instead, strongly mixed with the TiO_2 conduction band, with no level in this energy region having a N3 PDOS contribution exceeding 25%. This pair of ligand orbitals shows a more pronounced difference in coupling to the substrate as compared to the pairs of orbitals at −3.7 and −3.2 eV. Comparing the π_b*(−) orbital in Figure 3e and the π_a*(+) orbital in Figure 3g on the free dcb ligand, an explanation for the difference in coupling with TiO_2 can be that the π_a*(+) on the free dcb is further away from the substrate, in the sense that the π_a* symmetry of the pyridine rings means that there are no contributions to this orbital from the nitrogen atoms that effectively provide a through bond pathway for electronic coupling to the substrate via the central Ru atom. For the corresponding orbitals on the anchoring dcb ligand, on the other hand, the π_a*(+) orbital (not shown) appears to be somewhat more strongly mixed as compared to the π_b*(−) orbital shown in Figure 3f, as judged from the main PDOS contributions. This is compatible with the fact that the π_a*(+) is located energetically in a position where the substrate DOS is higher than for the π_b*(−) orbital. It is, however, somewhat surprising that the coupling appears to be so strong for the anchored dcb despite the fact that it for symmetry reasons should not mix strongly with the carboxylate π_b* orbital.

Photoinduced Surface Electron Transfer. The crucial photoinduced charge separation in the dye-sensitized solar cells is accomplished at the dye−semiconductor interface.[1,2] Typically, ruthenium dyes absorb visible light by well-understood metal to ligand charge transfer (MLCT) excitations from the highest occupied Ru 4d orbitals to unoccupied π* orbitals on the substituted poly-pyridine ligands (dcb in N3).[47,48] If there is a sufficiently strong interaction between the excited dye π* levels and the TiO_2 substrate conduction band, the initial photoexcitation can be followed by an ultrafast electron transfer of the excited electron to the substrate conduction band and can suppress competing processes such as intramolecular thermalization.[49] Here, the efficiencies of the surface electron transfer from excitations to different unoccupied π* levels are estimated using a Newns−Anderson electron coupling model[50] in which the width of the splitting of the relevant dye molecular orbital as it interacts with the conduction band quasi-continuum is taken as an electron coupling strength that can be converted to an electron injection time.[39] The accuracy of this approach is likely to be somewhat limited by the finite size of the nanocrystal model, which results in finite spacing of the band levels. The following discussion is therefore limited to the order of magnitude estimates of electronic coupling strengths and associated injection times.

The strongest couplings found in the calculations are for unoccupied molecular orbitals on the surface binding ligand overlapping the substrate electronic bands. An example of such a strong interaction is given by the π_b*(−) level at −3.1 eV, contributing to LUMO + 14 in Figure 3f. As mentioned previously, these levels are estimated from the present calculations to have electronic coupling strengths of the order of 100 meV. In the Newns−Anderson electron coupling model, this is consistent with photoinduced electron injection from these levels into the conduction band on the order of 10 fs. This is in basic agreement with observations of sub-100 fs components of the ultrafast photoinduced electron transfer in several experiments on related systems (see, e.g., ref 8). The strong electronic coupling across the dye−substrate interface is also consistent with the discussions about the electronic coupling of dcb itself with TiO_2.[16,17]

TABLE 2: Excitation Energies (eV), Oscillator Strengths (*f*), Dominant Contribution, and Character for the First Three Excited Singlet States According to the TD-DFT Calculation

state	*E* (eV)	f	dominant contribution	character
S1	0.965	0.0047	38% (HOMO) → (LUMO + 1)	N3 MLCT
S2	1.077	0.0261	39% (HOMO) → (LUMO)	N3 MLCT
S3	1.137	0.000	46% (HOMO−1) → (LUMO)	N3 MLCT

Weakly coupled levels include both dye orbitals below the conduction band edge as well as some states overlapping the conduction band energetically, but physically far removed from the TiO_2. These levels have small or negligible observable coupling strengths. Estimating these weak couplings to be less than 10 meV is consistent with photoinduced electron-transfer times on the order of 100 fs or longer. The same qualitiative trends for the variations in electronic coupling and delocalization were seen for the corresponding HF PDOS in which electron-transfer properties in general, and the Newns−Anderson electronic coupling model in particular,[50] have frequently been discussed. Thus, there appears to be at least an order of magnitude difference in calculated electronic couplings between weakly and strongly mixed unoccupied dye orbitals that can be related to the order of magnitude differences in photoinduced electron transfer rates from different excited dye states involving those particular orbitals. The marked sensitivity of the electronic coupling on the energy matching between the excited dye states and the conduction band in the vicinity of the conduction band edge, discussed previously, is consistent with biphasic or multiexponential injection, where heterogeneous electron transfer from orbitals overlapping the conduction band on the binding ligand occurs on a time scale of ca. 10 fs and where there are comparatively slow components of heterogeneous electron transfer from levels localized on the dye and situated energetically below the conduction band edge.

To further investigate the nature of the lowest excited singlet states, a TD-DFT calculation of the first three singlet−singlet excitations was performed at the optimized ground-state geometry described previously, and the results are summarized in Table 2. According to the principal MO contributions listed in Table 2, the first three vertical excitations in the N3-$(TiO_2)_{38}$ system are all MLCT excitation in the dye with vertical excitation energies of 0.97, 1.08, and 1.14 eV, respectively. They also correspond well with the lowest excitations in the N3 dye itself, which from a calculation performed in the same way as for the combined system indicated that the three lowest vertically excited singlet states were MLCT states with energies of 0.92, 0.97, and 1.07 eV, respectively. Thus, according to the present calculations, the lowest energy excitations have very similar character and only display a minor shift of 0.05−0.10 eV toward lower energies. This supports the molecular orbital analysis of the states in the vicinity of the conduction band edge. Because of a combination of stabilization of the occupied orbitals and destabilization of unoccupied orbitals, significant blue-shifts of the dye excitations can be expected in the presence of solvents.[23,24] It is also unlikely that the present nanocrystal has a fully developed bulk band structure.[41] Both these factors can be expected to affect the position of the lowest excited states relative to the conduction band edge, and it will therefore be interesting to investigate as to what extent these factors influence the excitation processes of this and related dye-sensitized nanocrystal systems.

Conclusions

Structural and electronic interactions between the N3 ruthenium dye and the TiO_2 nanorystal have been investigated using

DFT and TD-DFT calculations. Direct comparisons of the present calculations to published experimental data on N3-sensitized TiO_2 systems must be made with caution, as limitations to the correspondence between published experiments and the current calculations can be expected, for example, due to the lack of a full excitation spectrum, the relatively small size of the nanocrystal, as well as the neglect of solvent and other environmental effects. It is, however, encouraging that the calculated properties appear to be reasonably consistent with available experimental information of, for example, photoinduced heterogeneous electron transfer.

Structurally, the present calculations indicate that both the dye and the nanocrystal make significant structural adjustments to accommodate favorable binding between the dye and the semiconductor, simultaneously involving more than one anchoring site. This may increase the number of dye−substrate contact points as compared to what has been considered in terms of simpler modeling that neglects full structural relaxations of the system.

The calculated electronic structure shows an alignment of the molecular orbitals of the N3 dye with the band structure of the semiconductor nanoparticle that is reasonable in the light of available experimental evidence on the system, with the dye HOMO located in the fundamental band gap of the substrate and the lowest few unoccupied molecular orbitals of the dye located in the vicinity of the conduction band edge. Interfacial electron coupling strengths have been estimated to vary strongly depending on the energy and location of particular dye orbitals involved. Estimating calculated electronic coupling strengths from the calculations, there appears to be an order of magnitude difference in injection times between excitations to dye states that are strongly and weakly coupled to the TiO_2 substrate, with the strongest couplings corresponding to injection times on the order of 10 fs.

The calculations provide a detailed theoretical understanding of the interactions between the molecular orbitals of the sensitizer with the electronic bands of the substrate that helps to rationalize experimental observations of ultrafast multiexponential photoinduced heterogeneous electron-transfer rates in these systems. The present investigation also provides a starting point for systematic studies of the interaction of ruthenium dyes with nanostructured semiconductor substrates, including both comparisons of different adsorption modes and differences in the interfacial electronic interactions with different dyes and oxides. It is therefore an important step toward computer-aided design of better dye-sensitized nanocrystal electrode interfaces.

Acknowledgment. The Göran Gustafsson Foundation and the Magnus Bergvall Foundation are gratefully acknowledged for financial support. P.P. also gratefully acknowledges the Villa Capri Foundation for generous support. The Swedish National Supercomputer Centre (NSC) is acknowledged for generous grants of computer resources. We thank Prof. Sten Lunell, Uppsala University, and Dr. Lars Ojamäe, Linköping University, for valuable discussions.

Supporting Information Available: Hartree−Fock total DOS and N3 PDOS. This material is available free of charge via the Internet at http://pubs.acs.org.

References and Notes

(1) Miller, R. J. D.; McLendon, G. L.; Nozik, A. J.; Schmickler, W.; Willig, F. *Surface Electron-Transfer Processes*; VCH Publishers: Weinheim, 1995.
(2) Hagfeldt, A.; Grätzel, M. *Chem. Rev.* **1995**, *95*, 49.
(3) Hagfeldt, A.; Grätzel, M. *Acc. Chem. Res.* **2000**, *33*, 269.
(4) Tachibana, Y.; Moser, J. E.; Grätzel, M.; Klug, D. R.; Durrant, J. R. *J. Phys. Chem.* **1996**, *100*, 20056.
(5) Hannappel, T.; Burfeindt, B.; Storck, W.; Willig, F. *J. Phys. Chem. B* **1997**, *101*, 6799.
(6) Heimer, T. A.; Heilweil, E. J.; Bignozzi, C. A.; Meyer, G. J. *J. Phys. Chem. A* **2000**, *104*, 4256.
(7) Asbury, J. B.; Hao, E.; Wang, Y.; Gosh, H. N.; Lian, T. *J. Phys. Chem. B* **2001**, *105*, 4545.
(8) Benkö, G.; Kallioinen, J.; Korppi-Tommola, J. E. I.; Yartsev, A. P.; Sundström, V. *J. Am. Chem. Soc.* **2002**, *124*, 489.
(9) Huber, R.; Moser, J. E.; Grätzel, M.; Wachtveitl, J. *J. Phys. Chem. B* **2002**, *106*, 6494.
(10) Willig, F.; Zimmermann, C.; Ramakrishna, S.; Storck, W. *Electrochim. Acta* **2000**, *45*, 4565.
(11) Kilså, K.; Mayo, E. I.; Brunschwig, B. S.; Gray, H. B.; Lewis, N. S.; Winkler, J. R. *J. Phys. Chem. B* **2004**, *108*, 15640.
(12) Galoppini, E. *Coord. Chem. Rev.* **2004**, *248*, 1161.
(13) Persson, P.; Bergström, R.; Lunell, S. *J. Phys. Chem. B* **2000**, *104*, 10348.
(14) Wang, Y.; Anderson, N. A.; Lian, T. *J. Phys. Chem. B* **2003**, *107*, 9434.
(15) Duncan, W. R.; Prezhdo, O. V. *J. Phys. Chem. B* **2005**, *109*, 365.
(16) Persson, P.; Lunell, S.; Bruhwiler, P. A.; Schnadt, J.; Södergren, S.; O'Shea, J. N.; Karis, O.; Siegbahn, H.; Mårtensson, N.; Bässler, M.; Patthey, L. *J. Chem. Phys.* **2000**, *112*, 3945.
(17) Schnadt, J.; Bruhwiler, P. A.; Patthey, L.; O'Shea, J. N.; Södergren, S.; Odelius, M.; Ahuja, R.; Karis, O.; Bässler, M.; Persson, P.; Siegbahn, H.; Lunell, S.; Mårtensson, N. *Nature* **2002**, *418*, 620.
(18) O'Regan, B.; Grätzel, M. *Nature* **1991**, *353*, 737.
(19) Grätzel, M. *Nature* **2001**, *414*, 338.
(20) Persson, P.; Bergström, R.; Ojamäe, L.; Lunell, S. *Adv. Quantum Chem.* **2002**, *41*, 203.
(21) Rensmo, H.; Lunell, S.; Siegbahn, H. *J. Photochem. Photobiol., A* **1998**, *114*, 117.
(22) Monat, J. E.; Rodriguez, J. H.; McCusker, J. K. *J. Phys. Chem. A* **2002**, *106*, 7399.
(23) Fantacci, S.; De Angelis, F.; Selloni, A. *J. Am. Chem. Soc.* **2003**, *125*, 4381.
(24) Guillemoles, J.-F.; Barone, V.; Joubert, L.; Adamo, C. *J. Phys. Chem. A* **2002**, *106*, 11354.
(25) Joubert, L.; Guillemoles, J.-F.; Adamo, C. *Chem. Phys. Lett.* **2003**, *371*, 378.
(26) De Angelis, F.; Fantacci, S.; Selloni, A. *Chem. Phys. Lett.* **2004**, *389*, 204.
(27) Stier, W.; Duncan, W. R.; Prezhdo, O. V. *Adv. Mater.* **2004**, *16*, 240.
(28) Rego, L. G. C.; Batista, V. S. *J. Am. Chem. Soc.* **2003**, *125*, 7989.
(29) Ishiwaki, T.; Inoue, H.; Makishima, A. *J. Mater. Sci.* **2000**, *35*, 1669.
(30) Redfern, P. C.; Zapol, P.; Curtiss, L. A. Rajh, T.; Thurnauer, M. C. *J. Phys. Chem. B* **2003**, *107*, 11419.
(31) De Angelis, F.; Tilocca, A.; Selloni, A. *J. Am. Chem. Soc.* **2004**, *126*, 15024.
(32) Shklover, V.; Ovchinnikov, Yu. E.; Braginsky, L. S.; Zakeruddin, S. M.; Grätzel, M. *Chem. Mater.* **1998**, *10*, 2533.
(33) Vittadini, A.; Selloni, A.; Rotzinger, F. P.; Grätzel, M. *J. Phys. Chem. B* **2000**, *104*, 1300.
(34) Persson, P.; Stashans, A.; Bergström, R.; Lunell, S. *Int. J. Quantum Chem.* **1998**, *70*, 1055.
(35) Persson, P.; Lunell, S. *Sol. Energy Mater. Sol. Cells* **2000**, *63*, 139.
(36) Odelius, M.; Persson, P.; Lunell, S. *Surf. Sci.* **2003**, *529*, 47.
(37) Haukka, M.; Hirva, P. *Surf. Sci.* **2002**, *511*, 373.
(38) Ramakrishna, S.; Willig, F.; May, V.; Knorr, A. *J. Phys. Chem. B* **2003**, *107*, 607.
(39) Persson, P.; Lunell, S.; Ojamäe, L. *Chem. Phys. Lett.* **2002**, *364*, 469.
(40) Stier, W.; Prezhdo, O. V. *J. Phys. Chem. B* **2002**, *106*, 8047.
(41) Persson, P.; Gebhardt, J. C. M.; Lunell, S. *J. Phys. Chem. B* **2003**, *107*, 3336.
(42) (a) Hay, P. J.; Wadt, W. R. *J. Chem. Phys.* **1985**, *82*, 270. (b) Wadt, W. R.; Hay, P. J. *J. Chem. Phys.* **1985**, *82*, 284. (c) Hay, P. J.; Wadt, W. R. *J. Chem. Phys.* **1985**, *82*, 299.
(43) Frisch, M. J.; Trucks, G. W.; Schlegel, H. B.; Scuseria, G. E.; Robb, M. A.; Cheeseman, J. R.; Montgomery, J. A., Jr.; Vreven, T.; Kudin, K. N.; Burant, J. C.; Millam, J. M.; Iyengar, S. S.; Tomasi, J.; Barone, V.; Mennucci, B.; Cossi, M.; Scalmani, G.; Rega, N.; Petersson, G. A.; Nakatsuji, H.; Hada, M.; Ehara, M.; Toyota, K.; Fukuda, R.; Hasegawa, J.; Ishida, M.; Nakajima, T.; Honda, Y.; Kitao, O.; Nakai, H.; Klene, M.; Li, X.; Knox, J. E.; Hratchian, H. P.; Cross, J. B.; Bakken, V.; Adamo, C.; Jaramillo, J.; Gomperts, R.; Stratmann, R. E.; Yazyev, O.; Austin, A. J.; Cammi, R.; Pomelli, C.; Ochterski, J. W.; Ayala, P. Y.; Morokuma, K.;

Voth, G. A.; Salvador, P.; Dannenberg, J. J.; Zakrzewski, V. G.; Dapprich, S.; Daniels, A. D.; Strain, M. C.; Farkas, O.; Malick, D. K.; Rabuck, A. D.; Raghavachari, K.; Foresman, J. B.; Ortiz, J. V.; Cui, Q.; Baboul, A. G.; Clifford, S.; Cioslowski, J.; Stefanov, B. B.; Liu, G.; Liashenko, A.; Piskorz, P.; Komaromi, I.; Martin, R. L.; Fox, D. J.; Keith, T.; Al-Laham, M. A.; Peng, C. Y.; Nanayakkara, A.; Challacombe, M.; Gill, P. M. W.; Johnson, B.; Chen, W.; Wong, M. W.; Gonzalez, C.; Pople, J. A. *Gaussian 03*, revision C.02; Gaussian, Inc.: Pittsburgh, PA, 2004.

(44) Cramer, C. J. *Essentials of Computational Chemistry—Theories and Models*; John Wiley & Sons: Ltd.: New York, 2002; p 252−253.

(45) Muscat, J.; Wander, A.; Harrison, N. M. *Chem. Phys. Lett.* **2000**, *342*, 397.

(46) Benkö, G.; Kallioinen, J.; Myllyperkiö, P.; Trif, F.; Korppi-Tommola, J. E. I.; Yartsev, A. P.; Sundström. V. *J. Phys. Chem. B* **2004**, *108*, 2862.

(47) Vlcek, A., Jr. *Coord. Chem. Rev.* **2000**, *200−202*, 933.

(48) Yeh, A. T.; Shank, C. V.; McCusker, J. K. *Science* **2000**, *289*, 935.

(49) Lanzafame, J. M.; Palese, S.; Wang, D.; Miller, R. J. D.; Muenter, A. A. *J. Phys. Chem.* **1994**, *98*, 11020.

(50) Muscat, J. P.; Newns, D. M. *Prog. Suf. Sci*. **1978**, *9*, 1.